Kinetic Mechanism of Damage Site Recognition and Uracil Flipping by *Escherichia coli* Uracil DNA Glycosylase†

James T. Stivers*

Center for Advanced Research in Biotechnology, Biotechnology Institute, University of Maryland, and the National Institute for Standards and Technology, 9600 Gudelsky Drive, Rockville, Maryland 20850

Krzysztof W. Pankiewicz and Kyoichi A. Watanabe

Codon Pharmaceuticals, Inc., 200 Perry Parkway, Gaithersburg, Maryland 20877

Received August 4, 1998; Revised Manuscript Received October 21, 1998

ABSTRACT: The DNA repair enzyme uracil DNA glycosylase (UDG) catalyzes hydrolytic cleavage of the *N*-glycosidic bond of premutagenic uracil residues in DNA by flipping the uracil base from the DNA helix. The mechanism of base flipping and the role this step plays in site-specific DNA binding and catalysis by enzymes are largely unknown. The thermodynamics and kinetics of DNA binding and uracil flipping by UDG have been studied in the absence of glycosidic bond cleavage using substrate analogues containing the 2′-α and 2′-β fluorine isomers of 2′-fluoro-2′-deoxyuridine (U^{β}, U^{α}) positioned adjacent to a fluorescent nucleotide reporter group 2-aminopurine (2-AP). Activity measurements show that DNA containing a U^{β} or U^{α} nucleotide is a 10^7-fold slower substrate for UDG ($t_{1/2} \approx 20$ h), which allows measurements of DNA binding and base flipping in the absence of glycosidic bond cleavage. When UDG binds these analogues, but not other DNA molecules, a 4−8-fold 2-AP fluorescence enhancement is observed, as expected for a decrease in 2-AP base stacking resulting from enzymatic flipping of the adjacent uracil. Thermodynamic measurements show that UDG forms weak nonspecific complexes with dsDNA ($K_D^{ns} = 1.5\ \mu$M) and binds ∼25-fold more tightly to U^{β} containing dsDNA ($K_D^{app} \approx 50$ nM). Thus, base flipping contributes less than ∼2 kcal/mol to the free energy of binding and is not a major component of the $>10^6$-fold catalytic specificity of UDG. Kinetic studies at 25 °C show that site-specific binding occurs by a two-step mechanism. The first step (E + S ↔ ES) involves the diffusion-controlled binding of UDG to form a weak nonspecific complex with the DNA ($K_D \approx 1.5-3\ \mu$M). The second step (ES ↔ E′F) involves a rapid step leading to reversible uracil flipping ($k_{max} \approx 1200\ s^{-1}$). This step is followed closely by a conformational change in UDG that was monitored by the quenching of tryptophan fluorescence. The results provide evidence for an enzyme-assisted mechanism for uracil flipping and exclude a passive mechanism in which the enzyme traps a transient extrahelical base in the free substrate. The data suggest that the duplex structure of the DNA is locally destabilized before the base-flipping step, thereby facilitating extrusion of the uracil. Thus, base flipping contributes little to the free energy of DNA binding but contributes greatly to specificity through an induced-fit mechanism.

Enzymes which catalyze reactions at specific sites in DNA are presented with the formidable problems of finding the specific site in a sea of nonspecific sites and then forming specific interactions such that the transition state for the reaction is stabilized. A general mechanism used to solve these problems is to couple the processes of recognition, binding, and catalysis by conformational changes in the enzyme or DNA. These conformational changes, which have been implicated in the reactions of restriction enzymes (*1*), methyl transferases (*2, 3*), and several DNA repair enzymes (*4, 5*) to name only a few examples, can provide additional intrinsic binding energy for the specific substrate and greatly enhance specificity and catalysis (*6*). Indeed, given the highly repetitive structure of DNA, and the short sequences with which enzymes may interact, it may not be possible for an enzyme to obtain the required specificity by forming specific interactions with the substrate in the absence of conformational changes. Thus, studies addressing the structure, stability, and kinetics of such induced distortions in the enzyme and DNA are essential for understanding specificity and catalysis.

A recent and novel enzyme−DNA interaction implicated in specificity and catalysis of several enzymes is DNA base flipping (i.e., the rotation of the sugar and base out of the DNA helix) (*7*−*9*). From structural studies on enzymes, base flipping may occur via the major groove, such as with the enzyme uracil DNA glycosylase (*10*), or the minor groove of DNA, as seen with cytosine-5 methyltransferase (*2*). This differs from spontaneous base-pair opening, for which computational studies suggest that bases can only be extruded from the major groove (*11*). Two general mechanisms for enzymatic catalysis of base flipping can be proposed: *passive* and *active*. For the passive mechanism, the enzyme merely

* Address correspondence to this author. Telephone: 301-738-6264. Fax: 301-738-6255.

† This work was supported by NIH Grant RO1 GM56834 (J.T.S.).

10.1021/bi9818669 CCC: $18.00
Published on Web 12/29/1998

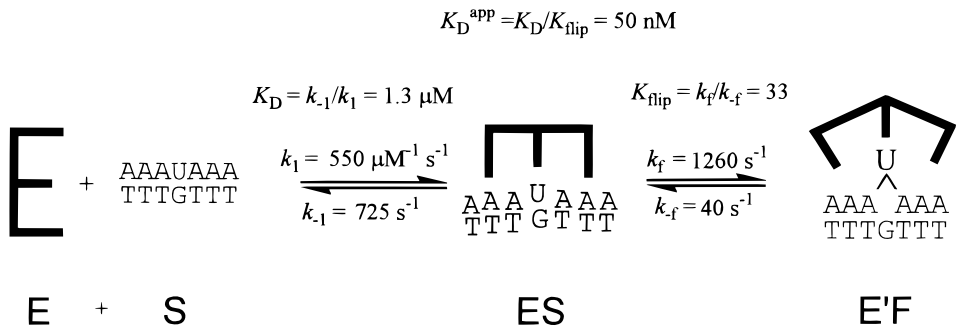

FIGURE 1: Minimal kinetic mechanism for damage site recognition by UDG. The rate constants are for **P**U$^{\beta}$A/TGT (see Table 1). The data indicate a two-step binding mechanism. The first step is the near diffusion-controlled association of UDG with the DNA to form a weak nonspecific encounter complex (ES). This complex rapidly isomerizes in the second step (k_f), resulting in uracil flipping and a conformational change in UDG that can be detected by transient changes in tryptophan fluorescence. As discussed in the text, the observed rate constant, k_f, represents the overall rate-limiting step that leads to a stable flipped-out uracil base. This rate-limiting step could reflect isomerization of the ES complex or the actual extrusion of the uracil from its stacked position in the DNA helix. Thermodynamically, the base-flipping step contributes less than 2 kcal/mol to the free energy of binding. Therefore, this induced-fit conformational change is a highly specific gateway to the catalytic machinery of UDG.

serves as a thermodynamic trap for an extrahelical base that is formed spontaneously in the free DNA. In an active mechanism, the enzyme enhances base flipping by forming interactions with the DNA that facilitate or accelerate the extrusion of the base from the helix. Two related questions are whether a stable or short-lived base-flipped intermediate is formed and whether base flipping or the subsequent chemical step is rate-limiting for all steps leading to enzyme bound products. A detailed understanding of these questions requires not only structural approaches but also new solution methods to probe the kinetics and thermodynamics of the base-flipping step on enzymes.

One structurally well-characterized DNA repair enzyme that uses a base-flipping mechanism is uracil DNA glycosylase (UDG). This enzyme, which removes premutagenic uracil bases from double- and single-strand DNA, acts by a direct hydrolytic mechanism, cleaving the N-glycosidic bond between the uracil base and the deoxyribose of DNA. UDG is an ideal enzyme system to study base flipping for several reasons. First, as demonstrated in this paper, stable 2′-fluoro-2′-deoxyuridine substrate analogues are available which allow the study of base flipping in the absence of glycosidic bond cleavage. Second, UDG can remove uracil residues from both double- *and* single-stranded DNA with high specificity (*12*). Thus, it is possible to compare the reaction mechanism for substrates that have dramatically different base-stacking and base-pairing properties. Finally, crystal structures of the human, herpes virus, and *Escherichia coli* enzymes have been solved (*10*, *13*−*15*).[1] The structure of the human UDG complexed with the products abasic DNA and uracil suggests that UDG flips the uracil base and the deoxyribose out of the DNA *major groove* by "pinching" the phosphodiester backbone at the deoxyuridine nucleotide and thrusting the side chain of a conserved leucine into the minor groove (*10*, *15*). Thus, the base is pushed into a uracil-specific binding pocket where catalytically important interactions with the base and deoxyribose can occur (*10*, *15*). Therefore in a general sense, UDG follows the same pathway for base flipping as suggested for the spontaneous reaction (i.e., the base is extruded from the major groove). This allows comparisons to be made between the kinetics and energetics of the enzyme-mediated reaction and spontaneous base-pair opening, which has been studied extensively using NMR methods (*16*).

Here we describe a study of the kinetic mechanism of site recognition and uracil flipping by *E. coli* UDG using stable 2′-fluoro-2′-deoxyuridine substituted substrate analogues in which a fluorescent reporter group, 2-aminopurine (2-AP), is placed adjacent to the excised uracil. The results provide evidence for an enzyme-assisted mechanism for uracil flipping and exclude a mechanism in which the enzyme traps a transient extrahelical base in the free substrate (Figure 1). The data suggest that the duplex structure of the DNA is locally destabilized before the base-flipping step, thereby facilitating extrusion of the uracil. Base flipping contributes little to the free energy of DNA binding but contributes greatly to specificity through an induced-fit mechanism.

EXPERIMENTAL PROCEDURES

Phosphoramidite Synthesis. 1-[2-Deoxy-5-*O*-(4,4′-dimethoxytrityl)-2-fluoro-1-β-arabinofuranosyl]uracil was synthesized by reacting 1-(deoxy-2-fluoro-1-β-D-arabinofuranosyl)-uracil (*17*) with dimethoxytrityl chloride in dry pyridine according to established protocols (*18*). ^{1}H NMR ($CDCl_3$): δ 3.40−3.46 (m, 2H, H5′, 5″), 3.78 (s, 6H, 2 × CH_3O−), 3.95−4.00 (m, 1H, H4′), 4.38−4.46 (two dd, 1H, H3′, $J_{2',3'}$ = 2.50 Hz, $J_{3',4'}$ = 4.54 Hz, $J_{3',F}$ = 18.68 Hz), 4.91−5.13 (two dd, 1H, H2′, $J_{1',2'}$ = 4.00 Hz, $J_{2',F'}$ = 51.86 Hz), 5.56 (dd, 1H, H5, collapsed to d after addition of D_2O, $J_{5,6}$ = 8.20 Hz, $J_{5',NH}$ = 2.1 Hz), 6.23 (dd, 1H, H1′, $J_{1',F'}$ = 17.20 Hz), 6.68−7.43 (m, 13 H, trityl), 7.55 (dd, 1H, H6, $J_{6,F}$ = 1.81 Hz), 8.24 (bs, 1H, NH exchange).

1-[2-Deoxy-5-*O*-(4,4′-dimethoxytrityl)-2-fluoro-1-β-arabinofuranosyl]uracil 3′-*O*-[(2-cyanoethyl)-*N*,*N*-diisopropyl]-phosphoramidite was prepared by reacting the above dimethoxytrityl derivative (548 mg, 1 mmol) with 2-cyanoethyl-*N*,*N*-diisopropylchlorophosphoramidite (284 mg, 1.2 mmol) in dry CH_2Cl_2 (20 mL) containing diisopropylethylamine (417 mg, 3.2 mmol). The reaction mixture was stirred under nitrogen, and the progress of the reaction was followed by TLC [ethyl acetate−benzene (4:3, v/v) containing 10 vol %

[1] Xiao, G., et al. 1999, in press. High-resolution crystal structures of the *E. coli* enzyme and its complex with uracil have been solved at 0.94 and 1.24 Å resolution, respectively.

of triethylamine].[2] When the starting material disappeared, the mixture was diluted with benzene (150 mL), washed with 5% $NaHCO_3$ (2 × 75 mL), dried (Na_2SO_4), and concentrated in vacuo to give an oily residue which was purified by chromatography on a silica column with ethyl acetate−benzene (4:3, v/v), containing 10 vol % triethylamine. Each of the UV-absorbing fractions was checked by TLC (the contaminant, a 2-cyanoethyl-*N*,*N*-diisopropylhydrogenphosphonoamidite diastereomer, which eluted very closely with the slowly migrating diastereomer could be visualized with $AgNO_3$ spray). The noncontaminated UV-absorbing fractions were collected and concentrated in vacuo and dissolved in benzene (20 mL). The solution was extracted with water (5 mL), dried (Na_2SO_4), and concentrated to give a white foam as a mixture of faster and slower migrating diastereomers in a ratio of 3:1. ^{1}H NMR ($CDCl_3$): δ 1.12−1.65 [2 d, 12H, 2 × (CH_3)$_2$CH], 2.39 (t, 2H, CH_2CH_2CN), 3.30−3.61 [m, 6H, H5′, 5″, CH_2CH_2CN, 2 × (CH_3)$_2CH$], 4.09−4.11 (m, 1H, H4′), 4.42−4.64 (m, 1H, H3′), 4.95 and 5.15 (two m, 1H, H2′, $J_{2',F'}$ = 54.00 Hz), 5.53 (d, 1H, H5, $J_{5,6}$ = 8.15 Hz), 6.21 (dd, 1H, H1′, $J_{1',2'}$ = 3.9 Hz, $J_{1',F}$ = 18.11 Hz), 6.80−7.50 (m, 13H, trityl), 7.54 (dd, 1H, H6, $J_{6,F}$ = 1.80 Hz), 8.60 (bs, 1H, NH). ^{31}P NMR ($CDCl_3$): δ 151.9 (s) and 152.1 (s), slower and faster migrating isomers, respectively. The synthesis and characterization of the U^{α} phosphoramidite derivative has been previously reported (*19*); this derivative was a gift from Dr. John Orban.

Oligodeoxynucleotide Synthesis. Oligodeoxynucleotides were synthesized using an Applied Biosystems 390 synthesizer using standard phosphoramidite chemistry, except that the coupling times for addition of the fluorinated nucleoside phosphoramidites were increased to 10 min.[3] All other nucleoside phosphoramidites were purchased from Applied Biosystems or Glen Research (Sterling, VA). After synthesis and deprotection, the oligodeoxynucleotides were purified by anion exchange HPLC and desalted by gel filtration chromatography. The size, purity, and nucleotide composition of the DNA were assessed by denaturing polyacrylamide gel electrophoresis with visualization by ^{32}P radiolabeling or ethidium bromide staining and MALDI mass spectrometry. The concentrations were determined by UV absorption measurements at 260 nm, using the pairwise extinction coefficients for the constituent nucleotides (*20*). The oligodeoxynucleotides used in these studies are shown in Figure 2.

5′-^{32}P End-Labeling of Oligonucleotides. Oligonucleotides were 5′-^{32}P-end-labeled using [γ-^{32}P]ATP in the presence of T4 polynucleotide kinase, the reaction was quenched by heating at 70 °C for 15 min, and the fractional incorporation of the label was determined by resolving the [γ-^{32}P]ATP from the oligonucleotide-bound radioactivity on a denaturing 20% mass fraction polyacrylamide gel and quantifying the radioactivity using a Molecular Dynamics Storm 840 phosphorimager. The unincorporated label was then removed from the quenched reaction using a membrane-based spin column (Qiagen), and the purified DNA was dissolved in 2 mM Tris−HCl (pH 8.0) and 0.2 mM EDTA. The concentration of the DNA was determined by its specific activity.

Hybridization of Duplex DNA. Duplex DNA molecules (Figure 2) were hybridized from the respective single-strand oligonucleotides in TN buffer (10 mM Tris−HCl (pH 8.0), 60 mM NaCl and 0.1 mM EDTA). Samples were heated to 70 °C, followed by slow cooling to room temperature over at least 2 h. The duplexes were formed by using a 5% excess of the unlabeled strand such that all of the radiolabel (or 2-AP containing strand) was in the duplex form. This was confirmed by performing electrophoresis on a native 20% mass fraction polyacrylamide gel followed by visualization using autoradiography or ethidium bromide staining.

Purification of UDG. UDG from *E. coli* strain B was purified to >99% homogeneity using a T7 polymerase-based overexpression system as described (*21*). The expressed protein has been characterized by high-resolution X-ray crystallography and MALDI mass spectrometry: *m*/*z* (obsd) = 25 535; MW (calc) = 25 536 assuming posttranslational removal of the amino terminal methionine (*12*). The concentration of the enzyme was determined using the relationship A^{280} (1 mg/mL) = 1.5 (*22*).

Steady-State Fluorescence Measurements. Steady-state fluorescence emission spectra of the AP containing oligodeoxynucleotide samples were measured on a SPEX Fluoromax spectrofluorometer. The emission spectra were recorded over the wavelength range of 330−450 nm with an excitation wavelength of 310 nm. For the time-base scans, the emission was observed at 370 nm with sampling at intervals of 1 s. The spectral band-pass was generally 4 nm for the emission spectra.

Glycosidic Bond Cleavage Assay. The cleavage assay takes advantage of the fact that the abasic product of the UDG reaction is cleavable by piperidine and may be resolved from the 5′-^{32}-P-end-labeled substrate by denaturing gel electrophoresis (*23*). Reactions using 10 μL were run with substrate concentrations of 500 nM and [UDG] = 1 nM (see Figure 3). The reactions were quenched with 4 μL of 10 M piperidine at appropriate times. An equal volume of load buffer (95% mass fraction formamide, 0.05% vol fraction bromophenol blue, and 0.05% vol fraction xylene cyanol) was added to each quenched sample, and the abasic sites generated by the enzyme were thermally cleaved at 90 °C for 30 min. Each time point was analyzed by electrophoresis on a 20% mass fraction polyacrylamide gel containing 8 M urea, and the extent of cleavage was quantified using a Molecular Dynamics Storm 840 phosphorimager.

Dissociation Constants for DNA Binding. The dissociation constants for UDG binding to ss**P**U$^{\beta}$A, **P**U$^{\beta}$A/TGT, and **P**U$^{\beta}$A/TAT DNA were determined by titrating fixed concentrations of the fluorescent DNA with increasing amounts of UDG. The concentration of the DNA was set approximately equal to the K_D value for these experiments. An excitation wavelength of 315 nm was used to minimize background fluorescence from tryptophan residues of the enzyme, and 2-AP emission spectra in the range of 340−450 nm were collected. The binding data were fitted to eq 1 after subtracting the background fluorescence of UDG from

[2] Abbreviations: Tris−HCl, tris(hydroxymethyl)aminomethane; dU, deoxyuridine; EDTA, (ethylenedinitrilo)tetraacetic acid, disodium salt; 2-AP, 2-aminopurine; 2-FU, 2′-fluoro-2′-deoxyuridine nucleotide; MALDI, matrix-assisted laser desorption−ionization mass spectrometry; TLC, thin-layer chromatography.

[3] Certain commercial equipment, instruments, and materials are identified in this paper in order to specify the experimental procedure. Such identification does not imply recommendation or endorsement by the National Institute of Standards and Technology, nor does it imply that the material or equipment identified is necessarily the best available for the purpose.

A.

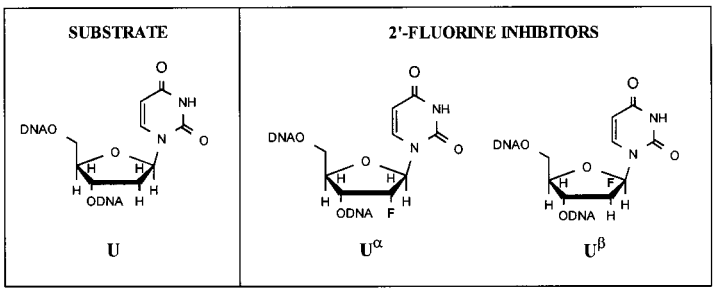

B.

Abbreviation	Oligonucleotide
I. Non-fluorescent oligonucleotides	
II. ssATA	5′ GCGGCCAAATAAAAAGCGC 3′
a.) AU$^{\beta}$A/TGT (X = U$^{\beta}$, Y = G)	5′ GCGGCCAAAXAAAAAGCGC 3′
b.) ATA/TAT (X = T, Y = A)	3′ CGCCGGTTTYTTTTTCGCG 5′
II. **P** opposite to site (2-AP^{opp})	
a.) AUA/T**P**T (X = U, U$^{\beta}$)	5′ GCGGCCAAAXAAAAAGCGC 3′
b.) A*F*A/T**P**T (X = *F*) [h]	3′ CGCCGGTTT**P**TTTTTCGCG 5′
c.) GU$^{\beta}$G/C**P**C (X = U$^{\beta}$)	
III. P adjacent to site (2-AP^{adj})	
a.) ss**P**XA (X = U$^{\beta}$, U$^{\alpha}$)	5′ GCGGCCAAPXAAAAAGCGC 3′
b.) **P**XA/TAT (X = U$^{\beta}$, U$^{\alpha}$, U^{r}, T)	5′ GCGGCCAAPXAAAAAGCGC 3′ 3′ CGCCGGTTTATTTTTCGCG 5′
c.) **P**XA/TGT (X = U$^{\beta}$, U$^{\alpha}$, C, T, *D*)	5′ GCGGCCAAPXAAAAAGCGC 3′ 3′ CGCCGGTTTGTTTTTCGCG 5′
d.) AU$^{\beta}$**P**/TGT	5′ GCGGCCAAAU$^{\beta}$ **P**AAAAGCGC 3′ 3′ CGCCGGTTTG TTTTTCGCG 5′
IV. Control (P two bases 3′ of U$^{\beta}$)	
a.) U$^{\beta}$A**P**/TTA	5′ GCGGCCAAAU$^{\beta}$ A**P**AAAGCGC 3′ 3′ CGCCGGTTTG TTTTTCGCG 5′

FIGURE 2: Substrates and 2′-fluoro-2′-deoxyuridine inhibitors of UDG. (A) The substitution at the 2′ position of an electron-withdrawing substituent such as fluorine is expected to greatly stabilize the glycosidic bond by increasing the positive charge on C-1′ in an oxycarbenium-ion transition state (Chart 1) for glycosidic bond hydrolysis (*28*). The U$^{\beta}$ fluorine isomer is otherwise similar to a 2′-H substituent with respect to the van der Waals radius (1.35 Å) and sugar pucker (C-2′ endo) (*46*, *47*). The U$^{\alpha}$ isomer has a C-3′ endo sugar pucker and is therefore more similar to RNA (*19*, *33*). (B) Sequences and abbreviations for the deoxyribonucleotide substrates and 2′-fluorine inhibitors of UDG. The nomenclature for the oligonucleotides reflects the 3 base sequence surrounding the central base on each strand. The nucleotides are listed in the 5′ to 3′ direction on each strand. Abbreviations: **P**, 2-aminopurine deoxyribonucleotide; U, uridine deoxyribonucleotide; U^{r}, uridine ribonucleotide; D, deoxyribose aldehyde abasic site; F, 3-hydroxy-2-(hydroxymethyl)tetrahydrofuran reduced abasic site analogue.

each spectrum (F_0 and F_f are the initial and final fluorescence intensities, respectively).

$$F = -\{(F_0 - F_f)/2 \times [\mathrm{DNA}]_{tot}\} \times \{b - (\sqrt{b^2 - 4[\mathrm{UDG}]_{tot}[\mathrm{DNA}]_{tot}})\} + F_0 \quad (1)$$

$$b = K_d + [\mathrm{UDG}]_{tot} + [\mathrm{DNA}]_{tot}$$

The dissociation constants for the nonfluorescent ATA/TAT and ssATA DNA molecules were determined by competitive displacement of 2-AP labeled DNA from UDG. For these experiments, a solution of 1.3 μM UDG and 1 μM ss**P**U$^{\beta}$A was titrated with increasing amounts of nonfluorescent competitor DNA (0−128 μM). The fluorescence emission intensities at 370 nm as a function of the total added ligand concentration were fit by computer using the program *DynaFit* (*24*), using the known dissociation constant for the fluorescent ss**P**U$^{\beta}$A DNA and the chemical equations for competitive binding of two ligands to a single site.

Stopped-Flow Kinetic Measurements. Stopped-flow fluorescence experiments were performed at 25 °C in TN buffer using an Applied Photophysics device in the two-syringe mode (dead time = 1.1 ms). The dissociation and association kinetics were followed using 2-AP or tryptophan fluorescence changes and were fit as single exponentials at all concentrations investigated, with no discernible bursts or lags ($F_t = \Delta F \exp(-k_{obsd}t) + C$, where F_t is the fluorescence at time t, ΔF is the total amplitude of the fluorescence change, and C is a constant offset). 2-AP containing DNA was excited at 310 nm, and the fluorescence emission was monitored

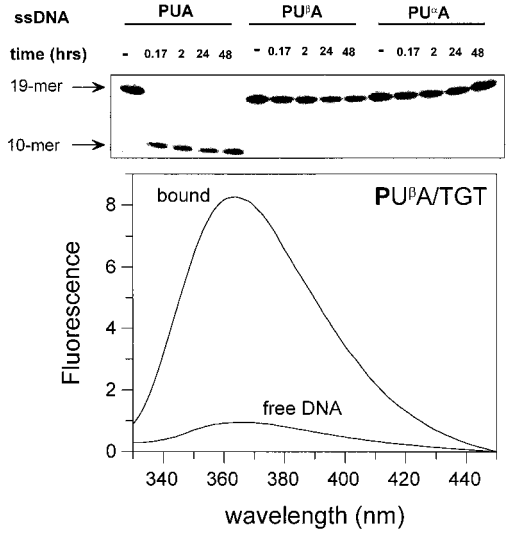

FIGURE 3: Cleavage assay for enzymatic processing of ss**P**UA, ss**P**U$^{\beta}$A, and ss**P**U$^{\alpha}$A 19-mers and fluorescence assay for uracil flipping. (Upper panel) 5′-^{32}P-end-labeled DNA concentrations (500 nM) and UDG concentration (1 nM). (Lower panel) Fluorescence enhancement of the 2-AP probe when UDG (0.98 μM) binds **P**U$^{\beta}$A/TGT DNA (0.5 μM). The background fluorescence of the enzyme was subtracted from the spectrum for the complex.

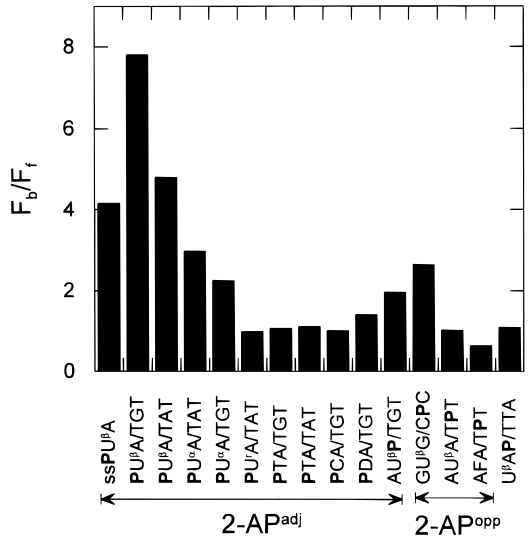

FIGURE 4: Fluorescence changes when UDG binds 2-AP labeled DNA oligonucleotides (TN buffer, 25 °C). The ratios of the fluorescence emission intensities of the bound (F_b) and free (F_f) DNA are plotted (λ_{em} = 370 nm and λ_{ex} = 310 nm). Only the U$^{\beta}$ and U$^{\alpha}$ inhibitors show large enhancements upon binding the enzyme. The largest enhancements for U$^{\beta}$ are seen when 2-AP is placed on the 5′ side of the uracil base. The control DNA (U$^{\beta}$A**P**/TTA), with 2-AP located two bases 3′ to the uracil, shows no fluorescence enhancement upon binding to UDG. Thus, the observed enhancements are due to disruption of 2-AP base stacking with the directly adjacent uracil as it flips into the enzyme active site.

using a 360-nm cut-on filter. For tryptophan fluorescence measurements, excitation was at 290 nm, and the fluorescence emission was monitored using a 335-nm cut-on filter. Typically, 10−15 kinetic traces were averaged to increase the signal-to-noise ratio. All bimolecular association reactions were performed under pseudo-first-order conditions with one reactant, either the enzyme or DNA, provided in at least a 5-fold excess over the limiting reactant. Other specifics of the individual reactions are described in the figure legends and text.

Estimating the Microscopic Kinetic Parameters for Two-Step Binding. An estimation of the microscopic rate constants for two-step binding (Figure 1) requires knowledge of the relative fluorescence intensities of each species (i.e., S, ES, and E′F) and the assignment of a minimal kinetic mechanism. In the analysis used here, the increase in fluorescence intensity upon DNA binding is assigned entirely to the E′F complex. This assignment is based on three observations. First, none of the nonspecific ES complexes between UDG and 2-AP labeled DNA show any significant fluorescence change (see Figure 4). Second, at 5 °C, the amplitude of the fluorescence change for **P**U$^{\beta}$A/TGT is equal to the 8-fold increase seen in the steady-state fluorescence emission spectra. If a significant quenching or enhancement of the 2-AP fluorescence occurred upon formation of the ES complex, then it would have been detected in this experiment, because the reaction rate is about 6-fold slower at this temperature (not shown). Finally, the dissociation of E′F is monophasic, once again suggesting that the fluorescent increase is due to a single enzyme-bound fluorescent species (see Figure 8).

The concentration dependence of the observed binding rates (k_{obsd}; see Figure 7C) were fitted to eq 2, where the

$$k_{obsd} = \frac{k_1[S](k_{-f} + k_f) + k_{-1}k_{-f}}{k_1[S] + k_{-1} + k_{-f} + k_f} \quad (2)$$

rate constants correspond to the mechanism in Figure 1 (*25, 26*). In principle, this two-step mechanism should show double-exponential kinetics, with a lag in EF formation at substrate concentrations in which the rates of association and dissociation (k_1[E] and k_{-1}) are comparable to the forward rate of conversion of ES to EF ($k_f + k_{-f}$) (*25, 26*). *However, single-exponential kinetics and a hyperbolic concentration dependence of k_{obsd} (eq 2) will be observed when the sum of the rate constants k_1[E], k_{-1}, k_f, and k_{-f} are larger than the time resolution of the measurement method* (*25*). Indeed, for the studies described here, this sum is large (>1700 s^{-1}), and a lag or second exponential term is not observed at any UDG concentration. An alternative rapid equilibrium mechanism (where $k_{-1} \gg k_f$) is not compatible with the data because the dissociation rates (k_{-1}) are similar to k_f (see Table 1).

The concentration dependence of the observed rates of binding were fit to eq 2 using the curve-fitting program *GraFit 4.0* to obtain the observed on-rate [$k_{on} = k_1k_{max}/(k_{-1} + k_{max})$], the observed off-rate [$k_{off} = k_{-1}k_{-f}/(k_{max} + k_{-1})$], and the maximal rate ($k_{max} = k_f + k_{-f}$) (*27*). In addition, the raw kinetic traces and the concentration dependence of the binding data were simulated by numerical integration using the programs *Kinsim* and *Fitsim* (*28, 29*). The method for estimating the microscopic kinetic parameters is described in the legend to Table 1. The reported uncertainties in the microscopic kinetic constants are estimated maximum errors obtained from trial and error simulations of the individual kinetic traces and the best-fit values from curve fitting to eq 2.

RESULTS AND DISCUSSION

2′-Fluorodeoxyuridine Analogues Are Not Substrates for UDG but Do "Flip". To study base flipping in isolation, it

Table 1: Thermodynamic and Kinetic Parameters for Nonspecific DNA Binding and 2′-Fluoro-2′-Deoxyuridine Containing DNA Binding to *E. coli* Uracil DNA Glycosylase[a]

measured rate constants[b]	**P**U$^{\beta}$A/TGT	**P**U$^{\beta}$A/TAT	ss**P**U$^{\beta}$A	ATA/TAT	ssATA
k_{on} (s^{-1})	360 ± 20	320 ± 50	250 ± 50		
k_{off} (s^{-1})	20 ± 2	28 ± 2	42 ± 3		
$k_{max} = k_f + k_{-f}$ (s^{-1})	1300 ± 100	1200 ± 200	1300 ± 100		
K_D^{app} (μM)[c]	0.05 ± 0.02	0.08 ± 0.02	0.140 ± 0.02		
k_{off}/k_{on} (μM)	0.055 ± 0.01	0.09 ± 0.02	0.17 ± 0.04		
$K_D^{ns} = k_{-1}/k_1$ (μM)[d]				1.5 ± 0.2	3.1 ± 1
microscopic rate constants[e]	**P**U$^{\beta}$A/TGT	**P**U$^{\beta}$A/TAT	ss**P**U$^{\beta}$A	ATA/TAT	ssATA
k_1 (μM^{-1} s^{-1})	550	420	500		
k_{-1} (s^{-1})	725	680	790		
k_f (s^{-1})	1260	1140	1200		
k_{-f} (s^{-1})	40	60	100		
K_{flip} (k_f/k_{-f})	33	19	12		
K_D (k_{-1}/k_1) (μM)	1.3	1.6	1.6	1.5 ± 0.2	3.1 ± 1

[a] T = 25 °C and pH 8.0. [b] The measured rate constants k_{on}, k_{off}, and k_{max} are related to the microscopic rate constants in Figure 1 using the analytical expression for two-step binding (eq 2) (*25, 26*). [c] K_D^{app} is the overall equilibrium constant for the two-step binding mechanism shown in Figure 1 (i.e., $K_D^{app} = K_D/K_{flip} = k_{off}/k_{on}$). [d] The thermodynamic dissociation constant (K_D^{ns}) for nonspecifically bound DNA is indistinguishable from the estimated value for $K_D = k_{-1}/k_1$ for the ES complex in Figure 1 (see below). [e] The estimated microscopic rate constants correspond to the two-step mechanism shown in Figure 1. The value for k_{on} is near the diffusion-controlled limit (k_{dif}) (*36*) and is temperature-*independent* in the range of 25−35 °C (not shown). Thus, this result indicates that $k_1 \approx k_{on} \approx k_{dif}$. A best-fit value for k_1 was obtained by curve fitting to eq 2 (see below). The value for K_{flip} was calculated from the measured K_D^{app} and the measured dissociation constant (K_D^{ns}) for nonspecific DNA binding ($K_{flip} = K_D^{app}/K_D^{ns}$). Through use of this value for K_{flip}, the individual values for k_f and k_{-f} were calculated by simultaneous solution of the two equations $K_{flip} = k_f/k_{-f}$ and $k_{max} = k_f + k_{-f}$. The values for k_{-1} were calculated as follows. Computer simulation of the off-rate data [$k_{off} = k_{-1}k_{-f}/(k_{max} + k_{-1})$] was first used to obtain an estimate of the product $k_{-1}k_{-f}$ for each substrate analogue (values for $k_{-1}k_{-f}$ of 29 000 ± 7000, 41 000 ± 8000, and 64 000 ± 15 000 s^{-2} were estimated for the **P**U$^{\beta}$A/TGT, **P**U$^{\beta}$A/TAT, and ss**P**U$^{\beta}$A analogues, respectively). Thus, an estimate for k_{-1} could be obtained by dividing the product $k_{-1}k_{-f}$ by k_{-f}. These values for k_{-1} are in reasonable agreement with estimates obtained by competition off-rate experiments using nonspecific DNA (see text). The final best-fit values were obtained from curve fitting the concentration dependence of k_{obsd} to eq 2 using the constraints on the individual rate constants obtained from simulations and the thermodynamic measurements. We estimate that the uncertainties in k_1, k_{-1}, k_f, and k_{-f} are less than 40%.

is necessary first, to develop a strategy to prevent the subsequent bond cleavage step and, second, to detect the flipping event. The approach taken here was to use 2′-fluorine substituted uridine analogues to prevent glycosidic bond cleavage (U$^{\beta}$, U$^{\alpha}$; Figure 2A) and to incorporate a fluorescent 2-AP base adjacent to the uracil to detect the flipping event. This two-pronged approach centers on the facts that (i) electron-withdrawing groups at the 2′ position are expected to destabilize an oxycarbenium ion transition state, thereby preventing glycosidic bond cleavage (Chart 1) (*30*), and (ii)

Chart 1

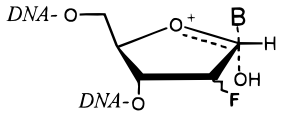

the 2-AP base should show a large fluorescence increase when the adjacent uracil flips from the helix because of a decrease in base stacking interactions that otherwise strongly quench its fluorescence (*31*).

As shown in Figure 3, when 500 nM 2-AP labeled ssDNA containing U, U$^{\beta}$, and U$^{\alpha}$ is incubated with 1 nM UDG for varying times and then analyzed using the abasic site cleavage assay, no cleavage products were observed for the fluorinated analogues even after 48 h under these limiting enzyme conditions. In contrast, the single-strand U substrate was processed almost completely in 10 min. In NMR experiments, where single-strand 2-FU$^{\beta}$ DNA was *stoichiometrically* bound to UDG, a half-life for cleavage of ∼20 h was estimated (not shown). Thus, the 2-FU$^{\beta}$ substrate analogue is ∼10^7-fold less reactive than the corresponding deoxyuridine substrate, which has a single-turnover cleavage rate of ∼150 s^{-1} (*32*). This half-life is 20−10 000-fold greater than the time scale of the thermodynamic and kinetic measurements reported below and allows for the study of DNA binding and base flipping in the absence of glycosidic bond cleavage.

To determine whether these chemically stable uridine analogues could flip into the UDG active site, steady-state fluorescence spectra were acquired. When a stoichiometric amount of UDG is mixed with the fluorescent **P**U$^{\beta}$A/TGT duplex, an 8-fold increase in 2-AP fluorescence is observed, consistent with the flipping of 2-AP out of the DNA helix (Figure 3). Somewhat smaller maximal fluorescence increases in the range of ∼2−5-fold were seen when UDG binds to other U$^{\beta}$ and U$^{\alpha}$ constructs (Figure 4). These include constructs with U$^{\beta}$/A, U$^{\beta}$/G, and U$^{\beta}$/**P** base pairs, as well as sequences where U$^{\beta}$ is flanked on both sides by G and on the 3′ side by 2-AP. Interestingly, both U$^{\alpha}$/A and U$^{\alpha}$/G constructs show a fluorescence increase, indicating that nucleotides such as these, with a ribose-like 3′-endo sugar pucker, can also be flipped by UDG (*19, 33*). However, UDG apparently cannot flip a uridine ribonucleotide (U^{r}) from an otherwise DNA duplex (see **P**U^{r}A/TAT in Figure 4). This result suggests that it is the steric constraints imposed by the 2′-hydroxyl, and not the ribose sugar pucker, which prevent the ribonucleotide from forming a stable flipped-out species.

To further investigate whether this UDG dependent fluorescence increase was due to uracil flipping and not to an unrelated fluorescence enhancement, the U adjacent to the 2-AP base was changed to T, C, a tetrahydrofuran abasic site (F), or a naturally occurring aldehydic abasic site (D). When the fluorescence intensities of these duplexes were

measured in the absence (F_f) and presence (F_b) of saturating concentrations of UDG, no significant fluorescence changes were observed (see F_b/F_f ratios in Figure 4). [It should be pointed out in this context that the abasic duplexes have a higher fluorescence intensity than the normal duplexes *before* UDG is added, because of decreased 2-AP base stacking. The small (≤35%) fluorescence changes that are observed for the abasic duplexes with 2-AP opposite and adjacent to the abasic site are not unexpected, because the human UDG has been shown to flip-out abasic sugar residues (*15*).] Importantly, a control duplex with 2-AP located two positions 3′ of U$^\beta$ also showed *no* fluorescence change upon binding to UDG (see U$^\beta$A**P**/TTA in Figure 4). Thus the enhancement requires that the 2-AP be initially stacked with the uracil or, to a lesser extent, base-paired with the uracil.

The large fluorescence intensities of the enzyme-bound **P**U$^\beta$A/TGT and **P**U$^\beta$A/TAT duplexes and ss**P**U$^\beta$A single-strand DNA suggest that the base-flipping equilibrium (K_{flip}) strongly favors the flipped-out base. Indeed, the fluorescence intensities of these three enzyme-bound DNA molecules are 10%, 7%, and 30%, respectively, of that for equimolar 2-AP riboside free in solution. The similar fluorescence intensities of ss**P**U$^\beta$A and free 2-AP riboside suggest that the 2-AP base of this ssDNA substrate analogue is largely unstacked from its neighboring bases when the uracil is flipped into the active site pocket. In contrast, the 2-AP base in the two duplex substrate analogues is still partially quenched because of the remaining base-stacking interactions on one face of the 2-AP. This is consistent with the crystal structures of several human UDG-product complexes, which show that the 5′-base adjacent to the flipped-out uracil is still stacked with its neighboring base (*10*, *15*).

What Is the Contribution of Uracil Flipping to the Free Energy of Binding? The large and specific fluorescence increase when UDG binds 2-AP labeled 2-FU$^\beta$ DNA provides a method to measure the contribution of uracil flipping to the thermodynamic stability of UDG−DNA complexes. As shown in Figure 5, binding of ss**P**U$^\beta$A by UDG can be monitored directly by following the increase in 2-AP fluorescence. Similar titrations were performed with duplex DNA constructs containing U/G and U/A base pairs (**P**U$^\beta$A/TGT and **P**U$^\beta$A/TAT), and the apparent dissociation constants for these oligonucleotides (K_D^{app}) are reported in Table 1. Once the dissociation constants for these fluorescent substrate analogues were determined, it was then possible to measure the dissociation constants for nonspecific DNA binding (K_D^{ns}) by competition experiments. For these measurements, nonfluorescent DNA without a deoxyuridine nucleotide was used (see ssATA and ATA/TAT in Figure 2 and Table 1). A representative competition binding experiment is shown in Figure 6, where a highly fluorescent complex between UDG and ss**P**U$^\beta$A is titrated with increasing concentrations of ATA/TAT nonspecific dsDNA. The K_D^{ns} values for ssATA and ATA/TAT are reported in Table 1.

From these thermodynamic studies, the binding affinity of UDG for DNA that contains a stable uracil base was found to be in the range of ∼50−140 nM, with K_D^{app} values in the relative order of U$^\beta$/G ≈ U$^\beta$/A < ssU$^\beta$. These dissociation constants for double- and single-strand U$^\beta$ substrate analogues are similar to the K_m values previously reported for double- and single-strand DNA substrates of UDG under similar conditions (*21*, *22*). The affinity of UDG for ds- and ssDNA without a uracil base (K_D^{ns}) was found to be in the low micromolar range, with ssDNA binding about 2-fold less tightly than dsDNA (Table 1). Thus, the U$^\beta$ substrate analogues that flip the uracil base from the helix bind ∼25-fold more tightly than the corresponding single-strand or duplex DNA molecules that lack the uracil. These modest differences in binding affinity correspond to a net free-energy

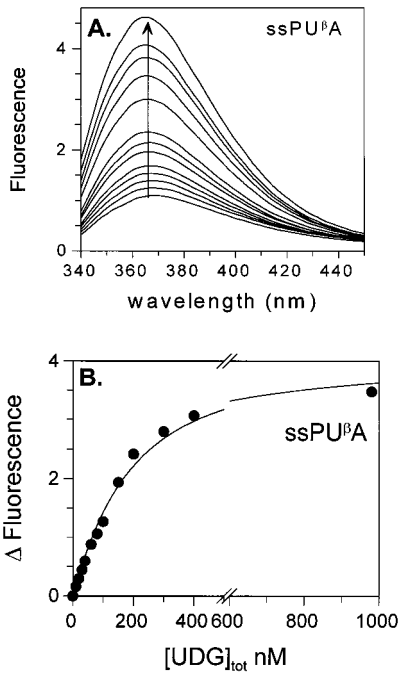

FIGURE 5: Determination of the dissociation constant for ss**P**U$^\beta$A using 2-AP fluorescence changes. (A) Changes in the fluorescence emission spectra of ss**P**U$^\beta$A DNA (80 nM) as a function of [UDG] (0−980 nM). (B) Change in fluorescence intensity at 370 nm as a function of total [UDG]. The line is a best fit to eq 1 (K_D^{app} = 0.14 ± 0.02 μM).

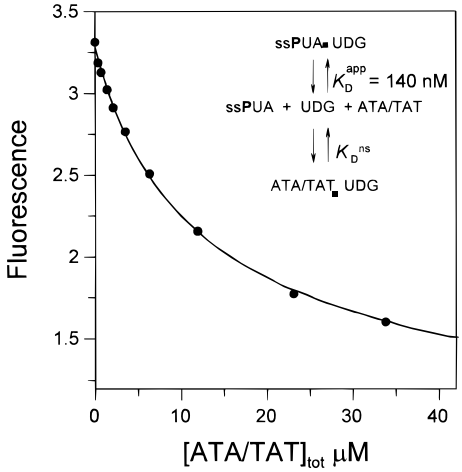

FIGURE 6: Determination of the dissociation constant for nonspecific DNA binding to UDG (K_D^{ns}) using a competitive fluorescence displacement assay. Increasing concentrations of ATA/TAT duplex 19-mer (0−34 μM) were added to a preformed complex of UDG (1.3 μM) and ss**P**U$^\beta$A (1 μM). The fluorescence intensity decrease at 370 nm due to the displacement of the 2-AP labeled single-strand DNA by the unlabeled competitor DNA is plotted. The data were fit by computer using the known dissociation constant for ss**P**U$^\beta$A (Figure 5 and Table 1) and the chemical equations for competitive binding using the program *DynaFit* (*24*). From this analysis, K_D^{ns} = 1.5 ± 0.2 μM.

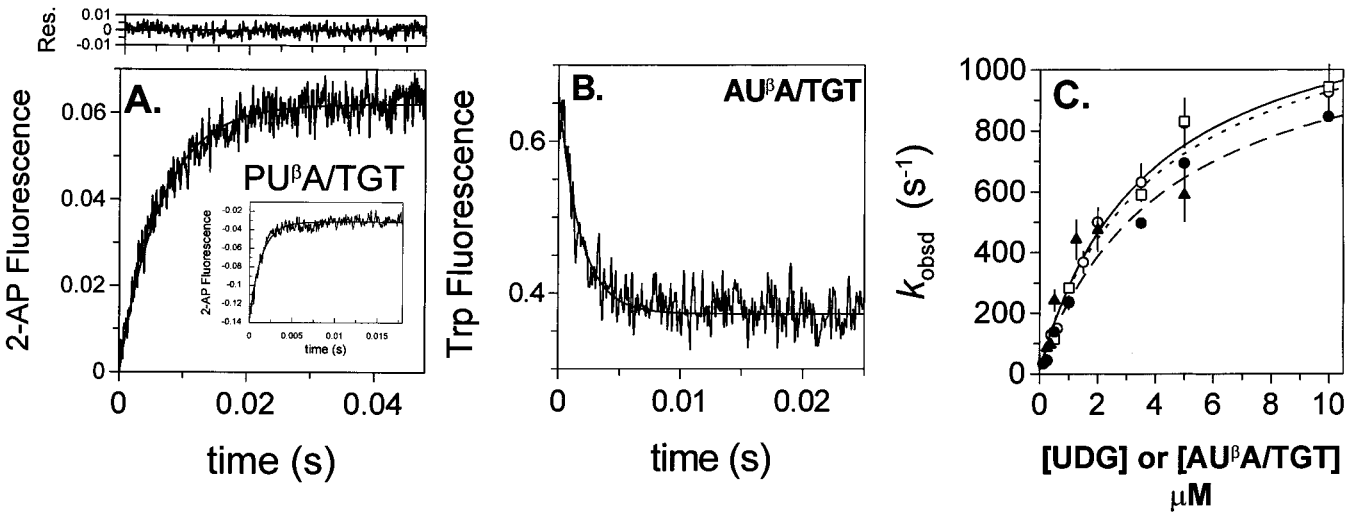

FIGURE 7: Binding kinetics for ss**P**U$^{\beta}$A, **P**U$^{\beta}$A/TGT, **P**U$^{\beta}$A/TAT, and AU$^{\beta}$A/TGT as determined by stopped-flow fluorescence measurements. (A) Kinetic trace for association of **P**U$^{\beta}$A/TGT (100 nM) with UDG (600 nM) using 2-AP fluorescence as the signal. The residuals for a single-exponential fit to the data are shown. To compare the quality of the data at a higher concentration of UDG, the inset shows an average of 13 kinetic traces obtained using 5 μM UDG and 500 nM **P**U$^{\beta}$A/TGT. (B) Kinetic trace for association of AU$^{\beta}$A/TGT (5 μM) with UDG (500 nM) using tryptophan fluorescence as the signal. The line is the best-fit to a single-exponential decay. (C) Concentration dependence of the observed rate constants for association of ss**P**U$^{\beta}$A (squares), **P**U$^{\beta}$A/TGT (open circles), **P**U$^{\beta}$A/TAT (closed circles), and AU$^{\beta}$A/TGT (triangles) with UDG. The error bars represent the standard deviation of at least three replicate measurements of the indicated rate constant; the other measured rates showed similar errors. The k_{obsd} values for AU$^{\beta}$A/TGT were obtained by monitoring the change in tryptophan fluorescence; the other values were measured by following 2-AP fluorescence changes. The curves are obtained from eq 2 using the kinetic parameters reported in Table 1.

contribution of less than 2 kcal/mol that may be attributed to uracil flipping. Because UDG has a lower-limit catalytic-specificity ratio $(k_{cat}/K_m)^U/(k_{cat}/K_m)^{ns}$ of greater than 10^6, this thermodynamic effect is not a major contribution to the enormous catalytic specificity of UDG.[4]

These dissociation constants for U$^{\beta}$/G and U$^{\beta}$/A containing duplex DNA molecules are ~1 and $^1/_{26}$, respectively, of those recently reported for the herpes virus UDG (*35*) and $^1/_4$ of the K_d values of the human UDG for 4′-thio substituted substrate analogues containing U/G and U/A base pairs (*15*). In addition, association and dissociation rate constants in the range of $\sim 10^4-10^6$ M^{-1} s^{-1} and $\sim 0.03-0.05$ s^{-1}, respectively, have been reported for the viral and human enzymes. These values are 100−10 000-fold lower than those reported in Table 1 for the *E. coli* UDG (see Table 1 footnotes). In these studies of the viral and human enzymes, inactive mutants or 4′-thio substituted substrate analogues were used to prevent glycosidic bond cleavage, respectively, and binding was monitored using surface plasmon resonance methods. Thus, it is not clear whether these measurements reflect true mechanistic differences between the these UDGs or simply differences in the conditions of the experiments, the sequences of the DNA molecules, and the measurement methods. However, two conclusions can be made with respect to these discrepancies. First, the measured association rate constants for the viral and human enzymes are not kinetically competent to account for the steady-state k_{cat}/K_m value of $\sim 1 \times 10^8$ M^{-1} s^{-1} for the *E. coli* enzyme (*21*). Second, the off-rate of the human UDG from the abasic product ($k_{off} \approx 0.2$ s^{-1}) (*15*) is an order of magnitude too slow to account for the steady-state turnover number of the *E. coli* enzyme with duplex DNA substrates (~3 s^{-1}) (*21*). Finally, we are unable to detect UDG−DNA complexes by a gel electrophoretic mobility shift assay, even at micromolar concentrations of enzyme (not shown). This independent observation is consistent with the fast off-rates measured by stopped-flow methods for the *E. coli* enzyme (see below).

Association Kinetics and Uracil Flipping. Figure 7A shows the time course for the 2-AP fluorescence increase when **P**U$^{\beta}$A/TGT DNA is mixed with UDG in a stopped-flow fluorometer at 25 °C. The fluorescence change is monophasic and could be analyzed as a single-exponential process. Similar monophasic time courses were measured at other concentrations of UDG in the range of 0.25−10 μM. The k_{obsd} values show a hyperbolic concentration dependence for all of the substrates investigated (Figure 7C). This observation provides evidence for a minimal two-step binding mechanism involving a concentration-dependent association step to form a weak nonspecific encounter complex (ES), followed by a reversible concentration-independent isomerization of the ES complex to form a highly fluorescent species (see E′F in Figure 1).[5] Through the use of the analytical solution for a two-step reversible binding mechanism (eq 2), the initial linear slope of a hyperbolic plot of k_{obsd} against concentration provides an estimate of the on-rate $[k_{on} = k_1k_{max}/(k_{-1} + k_{max})]$, the *y* intercept approximates the observed off-rate $[k_{off} = k_{-1}k_{-f}/(k_{max} + k_{-1})]$, and the maximal rate ($k_{max} = k_f + k_{-f}$) is equal to the sum of the forward and reverse rate constants for formation of E′F (*25*, *26*).

[4] This lower-limit estimate of the catalytic specificity of UDG was obtained using the measured $k_{cat}/K_m = 100$ μM s^{-1} for the AUA/T**P**T substrate and the observation that no detectable cleavage of 5′-^{32}P-labeled duplexes at other positions was observed at long incubation times under conditions where >1% nonspecific cleavage could have been detected.

[5] A alternative mechanism in which the enzyme or DNA isomerizes *before* the association step is unlikely on the basis that the same binding kinetics are observed when the 2-AP fluorescence of the DNA or the tryptophan fluorescence of the enzyme is followed.

In general, for the **P**U$^{\beta}$A/TGT, **P**U$^{\beta}$A/TAT, and ss**P**U$^{\beta}$A analogues, k_{on} is diffusion-controlled ($\sim$300 μM s^{-1}), k_{off} is in the range of 20−40 s^{-1}, and k_{max} is $\sim$1200 s^{-1} (Table 1). The measurement of these comparatively large association rate constants using stopped-flow methods was made possible by the large 8-fold fluorescence increase due to base flipping (Figure 3) and by the use of micromolar concentrations of DNA, which serve to increase the observable signal. Despite these favorable conditions, at the highest UDG concentrations, where the observed rates approach $\sim$900 s^{-1} (see Figure 7C and insert in Figure 7A), only the last 37% of the reaction could be followed using our stopped-flow apparatus (dead time = 1.1 ms). The excellent agreement of the kinetically determined ratio, k_{off}/k_{on}, with the K_D^{app} values measured in the equilibrium binding experiments, provides an independent confirmation of the reliability of the kinetic measurements, because k_{off}/k_{on} must equal the overall thermodynamic dissociation constant (K_D^{app}) measured in the equilibrium binding experiments (see Table 1). The methods used to estimate the microscopic rate constants in Table 1 and Figure 1 are detailed in the footnotes of Table 1.

The temperature dependence of k_{obsd} was investigated in the range of 5−35 °C with the finding that k_{on} is temperature-*independent* in the range of 25−35 °C and strongly dependent on temperature below 25 °C (k_{on} is about 6-fold slower at 5 °C than at 25 °C; data not shown). These interesting results indicate that the reaction is essentially diffusion-controlled at temperatures $\geq$ 25 °C (i.e., $k_{dif} \approx k_{on} \approx k_1$) and that a step with a large activation barrier becomes rate-limiting as the temperature is decreased. Because k_{on} is a composite rate constant comprised of k_1, k_{-1}, and k_{max} (see above), then one, or more than one, of these steps may have a substantial activation barrier. A detailed investigation of the temperature dependence of the binding kinetics and thermodynamics will be reported elsewhere (Stivers, J. T., unpublished experiments).

We also discovered that the binding kinetics could be followed using changes in the tryptophan (trp) fluorescence of UDG. Although the identity of the trp residue(s) responsible for these changes is not known, the *E. coli* enzyme has six such residues, two of which, W141 and W164, are near the active site. Thus, when the nonfluorescent AU$^{\beta}$A/TGT analogue binds to UDG, a 1.8-fold decrease in the tryptophan fluorescence is observed under saturating conditions (not shown). This fluorescence change is *not* seen when normal duplex DNA binds to the enzyme (not shown). Thus, these steady-state fluorescence studies suggest that specific binding of dU-DNA alters the conformation of UDG. An alternative mechanism involving quenching of the fluorescence of these residues by the bound DNA is unlikely, because no direct DNA−tryptophan interactions are observed in the structure of the product complex of human UDG.

Figure 7B shows that the time course for the tryptophan fluorescence decreases when AU$^{\beta}$A/TGT DNA is mixed with UDG in a stopped-flow fluorometer at 25 °C. The k_{obsd} values determined by following tryptophan fluorescence also show a hyperbolic concentration dependence indistinguishable from that observed by following 2-AP fluorescence changes of the DNA (triangles in Figure 7C). In control stopped-flow experiments, we were unable to detect a fluorescence change upon mixing UDG with an identical duplex DNA without the 2-FU$^{\beta}$ nucleotide, indicating that this change is

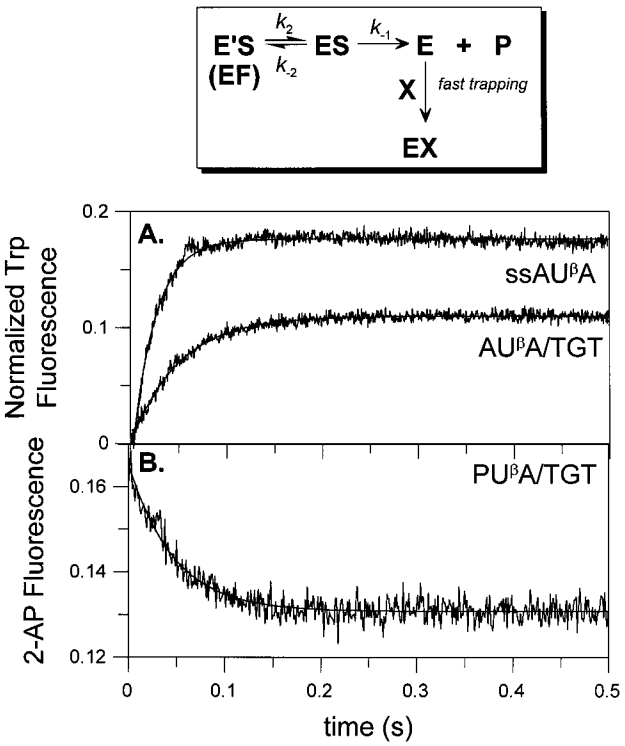

FIGURE 8: Dissociation kinetics of single-strand and duplex U$^{\beta}$ containing DNA followed using tryptophan or 2-AP fluorescence changes. (A) Double-strand DNA (100 μM) trap mixed with an equal volume solution containing either 0.5 μM UDG and 0.60 μM AU$^{\beta}$A/TGT or 1.0 μM UDG and 1.2 μM ssAU$^{\beta}$A. The time-dependent change in tryptophan fluorescence was then followed (λ_{ex} = 290 nm). (B) Double-strand DNA (100 μM) trap mixed with an equal volume solution containing 0.6 μM UDG and 0.5 μM **P**U$^{\beta}$A/TGT. The time-dependent change in 2-AP fluorescence was then followed (λ_{ex} = 310 nm). The curves are best-fits to a single-exponential decay (AU$^{\beta}$A/TGT and **P**U$^{\beta}$A/TGT k_{off} = 20 s^{-1}; ss**P**U$^{\beta}$A k_{off} = 42 s^{-1}).

specific for DNA containing a dU residue. The structural basis for these fluorescence changes is suggested by the crystal structure of the human UDG in complex with the reaction products abasic DNA and uracil. In this structure, a proline-rich active site loop containing the conserved His-187 and Leu-191 closes in on the bound substrate by $\sim$2 Å as compared to the position of this loop in the free enzyme (*10*). These structural changes upon 2-FU$^{\beta}$-DNA binding could affect the fluorescence properties of W141 or W164 by changing their environment.

Dissociation Kinetics. The observed dissociation rate of 2-FU$^{\beta}$ DNA from UDG (k_{off}) may be measured in a stopped-flow experiment by following the decrease in 2-AP fluorescence when a solution of UDG and 2-AP labeled 2-FU$^{\beta}$ DNA is mixed with a large molar excess of nonfluorescent competitor DNA (T) to make dissociation of the UDG−2-FU$^{\beta}$ DNA complex irreversible (Figure 8B). Alternatively, a solution of UDG and *nonfluorescent* 2-FU$^{\beta}$ DNA can be mixed with a large excess of competitor DNA, and the time-dependent increase in *tryptophan* fluorescence of UDG can be followed (Figure 8A). As seen for the association kinetics to form E′F, the k_{off} kinetics are also monophasic, and identical values for k_{off} were measured by following tryptophan or 2-AP fluorescence changes. As shown in Table 1, single-strand 2-FU$^{\beta}$ DNA dissociates as much as 2-fold more quickly than double-strand 2-FU$^{\beta}$ DNA, providing a quantitative explanation for the $\sim$2-fold weaker binding of

ss**P**U$^{\beta}$A DNA (Table 1). The identical k_{off} values measured by tryptophan fluorescence changes of UDG or 2-AP fluorescence changes of the DNA indicate that the same rate-limiting transition state is being observed for either signal. Thus, reinsertion of the uracil into the DNA helix is coupled with a conformational change in the enzyme. These off-rates measured by competition are in excellent agreement with those estimated from the *y* intercepts in Figure 8C by curve fitting to eq 2.

The ES Complex Is Indistinguishable from a Nonspecific UDG−DNA Complex. To discern the nature of the ES complex, we compared its calculated kinetic and thermodynamic properties with those directly measured for nonspecifically bound DNA. As described in detail in the footnote to Table 1, estimates of k_{-1} may be calculated from K_D^{app}, K_D^{ns}, and the product $k_{-1}k_{-f}$. These values for k_{-1}, which fall in the range of ∼500−1000 s^{-1}, are reported in Table 1. Thus, these calculations suggested that dissociation of the ES complex was rapid and that the observed $k_{off} = k_{-1}k_{-f}/(k_{max} + k_{-1})$ was limited by k_{-f} (i.e., $k_{-1} \gg k_{-f}$) (Figure 8).

To ascertain experimentally whether the dissociation rate (k_{-1}) of the ES complex was similar to that of nonspecifically bound DNA, competition dissociation experiments were performed with duplex ATA/TAT and ssATA DNA. In these stopped-flow experiments, a solution of ATA/TAT or ssATA DNA (2 μM) and UDG (1 μM) was mixed with an equal volume of fluorescent competitor ss**P**U$^{\beta}$A (10 μM). Thus, if binding and isomerization of ss**P**U$^{\beta}$A to E′F is fast compared to the off-rate of the nonspecifically bound DNA (k_{off}^{ns}), then the fluorescence should increase with a rate constant equal to k_{off}^{ns}. [Under these conditions, ∼40% of the enzyme is bound with ATA/TAT DNA at the time of mixing. Because of the small amount of free enzyme present and the rapid binding of ss**P**U$^{\beta}$A (Table 1), the kinetic phase expected from binding to the free enzyme is barely detectable in these experiments. Simulations confirmed this observation.] Through the use of this approach, respective k_{off} values for ATA/TAT and ssATA DNA of 440 and 540 s^{-1} were measured (data not shown). From simulations using the known kinetic parameters for ss**P**U$^{\beta}$A, we determined that the observed off-rates will underestimate the true k_{off}^{ns} by 11−67% as the true k_{off}^{ns} increases from 300 to 800 s^{-1}, that is, as k_{off}^{ns} approaches the trapping rate. Because the observed values are comparable to the trapping rate, then these values underestimate the true k_{off}^{ns} by about 27% and 40%. After the approximate corrections are made, k_{off}^{ns} values of ∼560 and ∼760 s^{-1} for ATA/TAT and SSATA DNA are calculated, respectively. These estimated values are in the same range as the calculated values for k_{-1} reported in Table 1. This experiment confirms that k_{off}^{ns} for nonspecifically bound DNA is rapid and indistinguishable from k_{-1} calculated for the ES complex. Therefore, the nonspecific and ES complexes are indistinguishable kinetically and thermodynamically (Table 1).

Mechanism of Uracil Flipping and Contribution to Specificity. Two general mechanisms for base flipping may be envisioned, a passive mechanism in which the enzyme captures a spontaneously flipped base in the free DNA or an active mechanism in which the enzyme facilitates base flipping. For UDG, enzymatic capture of a spontaneously flipped uracil is not a viable mechanism because this mechanism requires an association rate constant of *at least* 10^{11} M^{-1} s^{-1}, which is at least 10^2-fold faster than rates of diffusional encounter (*36*). This unrealistically high rate is required because the observed association rate of ∼4×10^8 M^{-1} s^{-1} (Table 1) must be normalized to account for the unfavorable equilibrium constant for base-pair opening in the *free* DNA ($K_{op} = 10^{-3}-10^{-6}$, see below). Direct evidence for an active mechanism is provided by the tryptophan fluorescence changes, which track with the kinetics of uracil flipping. These kinetic results are consistent with a concerted "pinch−push−pull" mechanism suggested by the crystal structures of human UDG bound to the reaction products uracil and abasic DNA (*10*, *15*). In the pinch part of this mechanism, the enzyme compresses the DNA phosphate backbone through interactions with a serine-rich loop (*15*). In the push part, the side chain of the conserved Leu-191 penetrates into the minor groove, assisting expulsion of the uracil. Finally, in the pull component, the uracil-specific hydrogen-bonding interactions in the recognition pocket are formed to specifically stabilize the flipped-out uracil. This induced-fit conformational change is not detected for nonspecifically bound DNA and provides a gateway to the catalytic machinery that only dU-DNA can unlock.

What Is the Initial Step in Damage Site Recognition by UDG? Several authors have suggested that base flipping alone is an inefficient initial damage recognition mechanism, because a substantial amount of binding energy and distortion of the duplex is required (*8*, *37*). Such considerations have led to the suggestion that damage recognition might proceed by a "processive extrusion" mechanism (*38*). In this mechanism, the enzyme migrates down the DNA, sequentially exchanging one extrahelical base for the next, in an isoenergetic exchange reaction, until the uracil is encountered and excised. The advantage of such a mechanism is that the enzyme need only pay the energetic penalty for conformational reorganization of the substrate *once* upon initial binding of the DNA.

Such a processive extrusion mechanism does not seem likely for UDG for several reasons. First, the fast off-rate of UDG from the nonspecific ES complex indicates that the enzyme has a relatively short residence time on the DNA and that a processive search mechanism could not operate over a significant length of DNA unless the sliding rate was exceedingly fast compared to this off-rate. Accordingly, previous processivity measurements of the *E. coli* UDG tend to show that the enzyme is not processive over long distances in the presence of physiological concentrations of salt (*39*−*41*). Second, the processive extrusion mechanism suggests that the enzyme flips *all* bases. However, the fluorescence data in Figure 4 provide no evidence that UDG flips any base other than uracil to a detectable extent. This observation is consistent with the structure of the UDG active site, which is exquisitely complementary to the uracil base and cannot readily accommodate any other base. Finally, the kinetic data presented here do not *require* linear diffusion on the DNA, because the rate of formation of the ES complex is simply that for diffusional encounter. However, these arguments do not exclude a "hopping" mechanism in which binding of UDG to one site on the DNA increases the probability of binding to a nearby site (*42*, *43*).

The data suggest that UDG pays the energetic cost for flipping the uracil base by deforming the duplex *before* the base-flipping step. This destabilization could occur at either

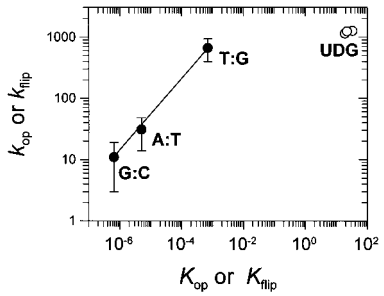

FIGURE 9: Linear free-energy relationships for the rates (k_{op}) and equilibria (K_{op} = [open]/[closed]) for spontaneous base-pair opening of G/C, A/T, and G/T base pairs as determined by NMR imino proton exchange studies (closed circles) at 25 °C and for UDG assisted uracil flipping (open circles). The data for spontaneous base-pair opening are from ref *16*, and the error bars represent the range of values obtained for these base-pair types in other studies (*44*−*46*). Thus, for spontaneous base-pair opening, the opening rates vary inversely with the stability of the base pair. For UDG, there is no dependence of the observed rate of base flipping (k_f) on the equilibrium constant (K_{flip}), suggesting that the energetic cost for base flipping has been paid for before the uracil-flipping step (see text and Figure 1).

of the two steps in the mechanism shown in Figure 1. In the first possible destabilization mechanism, the enzyme distorts the DNA upon formation of the initial nonspecific encounter complex (ES), followed by the rate-limiting uracil-flipping step (k_f). This mechanism is supported by the weak binding of DNA in the ES complex and the observation that k_f and K_{flip} are essentially the same for U^{β}/A, U^{β}/G, and ssU^{β} substrate analogues (Table 1). Thus, these analogues behave identically even though they would be expected to have significantly different energetics for base flipping (see below).[6] In the alternative mechanism, the enzyme destabilizes the DNA in the second step (k_f). In this case, k_f represents the rate-limiting isomerization (distortion) of the ES complex, followed by a much faster uracil-flipping step that is not directly detected. In either mechanism, the DNA is destabilized *before* the flipping step, leading to the observed independence of k_f from base-pair stability.

This result is shown in Figure 9 as a linear free-energy relationship, in which log k_f is plotted against log K_{flip} for the U^{β}/A, U^{β}/G, and ssU^{β} analogues. This plot of the rates and equilibria for enzymatic base flipping shows that there is no correlation between the base-pair stability of the DNA substrate and the rate of base flipping. This enzymatic result differs considerably from the process of spontaneous base-pair opening, as detected by imino proton exchange (*16*). For the spontaneous reaction, the rates (log k_{op}) and equilibrium constants (log K_{op}) for base-pair opening vary linearly with the stability of the base pair as shown in Figure 9 for G/C, A/T, and T/G base pairs (*16*, *44*−*46*). In further support of enzymatic destabilization of the bound DNA, several recent crystal structures of UDG−DNA complexes show a local compression of the phosphate−phosphate distance flanking the flipped-out nucleotide, leading to bending of the DNA. Because normal B DNA is not readily accommodated in the DNA binding cleft of UDG (*15*),[1] these structural results suggest that nonspecific DNA complexes may be similarly compressed and bent, thereby facilitating base flipping (*10*, *15*). Phosphate compression also is observed in the crystal structure of the related mismatch-specific UDG from *E. coli* (*48*), suggesting that this may be a general mechanism for detection of this type of DNA lesion.

[6] The melting temperatures of the corresponding U/A and U/G substrates differ by 2.2 °C (57.0 ± 0.2 and 54.8 ± 0.2 °C, respectively).

CONCLUSION

The kinetic and structural results suggest an active mechanism for uracil flipping by UDG involving (i) localized destabilization of the DNA helix upon binding, (ii) fast base flipping accompanied by an induced-fit conformational change in UDG, and (iii) stabilization of the extrahelical uracil by formation of specific hydrogen bonds with the enzyme. Because uracil flipping contributes <2 kcal/mol to the free energy of binding, we suggest that the $>10^6$-fold catalytic specificity of UDG is due to transition-state stabilization, with the intrinsic binding energy derived from this induced-fit conformational change.

REFERENCES

1. Winkler, F. K., Banner, D. W., Oefner, C., Tsernoglou, D., Brown, R. S., Heathman, S. P., Bryan, R. K., Martin, P. D., Petratos, K., & Wilson, K. S. (1993) *EMBO J. 12*, 1781−1795.
2. Klimsaukas, S., Kumar, S., Roberts, R. J., & Cheng, X. (1994) *Cell 76*, 357−369.
3. Reinisch, K. M., Chen, L., Verdine, G. L., & Lipscomb, W. N. (1995) *Cell 82*, 143−153.
4. Vassylyev, D. G., Kashwagi, T., Mikami, Y., Ariyoshi, M., Iwai, S., Ohtsuka, E., & Morikawa, K. (1995) *Cell 83*, 773−782.
5. Mol, C. D., Kuo, C.-F., Thayer, M. M., Cunningham, R. P., & Tainer, J. A. (1995) *Nature 374*, 381−386.
6. Herschlag, D. (1988) *Bioorg. Chem. 16*, 62−96.
7. Roberts, R. J. (1995) *Cell 82*, 9−12.
8. Cheng, X., & Blumenthal, R. M. (1996) *Structure 4*, 639−645.
9. Nelson, H. C. M., & Baker, T. H. (1996) *Chem. Biol. 3*, 419−423.
10. Slupphaug, G., Mol, C. D., Kavli, B., Arvai, A. S., Krokan, H. E., & Tainer, J. A. (1996) *Nature 384*, 87−92.
11. Ramstein, J., & Lavery, R. (1988) *Proc. Natl. Acad. Sci. U.S.A. 85*, 7231−7235.
12. Mosbaugh, D. W., & Bennett, S. E. (1994) *Prog. Nucleic Acid Res. Mol. Biol. 48*, 315−371.
13. Mol, C. D., Arvai, A. S., Slupphaug, G., Kavli, B., Alseth, I., Krokan, H. E., & Tainer, J. A. (1995) *Cell 80*, 869−878.
14. Savva, R., McAuley-Hecht, K., Brown, T., & Pearl, L. (1995) *Nature 373*, 487−493.
15. Parikh, S. S., Mol, C. D., Slupphaug, G., Bharti, S., Krokan, H. E., & Tainer, J. A. (1998) *EMBO J. 17*, 5214−5226.
16. Moe, J. G., & Russu, I. M. (1992) *Biochemistry 31*, 8421−8428.
17. Watanabe, K. A., Reichman, U., Hirota, K., Lopez, C., & Fox, J. J. (1979) *J. Med. Chem. 22*, 21−24.
18. Gait, M. J. (1984) *Oligonucleotide Synthesis*−*A Practical Approach*, IRL Press: Washington, DC.
19. Kawasaki, A. M., Casper, M. D., Freier, S. M., Lesnik, E. A., Zounes, M. C., Cummins, L. L., Gonzalez, C., & Cook, P. D. (1993) *J. Med. Chem. 36*, 831−841.
20. Fasman, G. D., Ed. (1975) *Handbook of Biochemistry and Molecular Biology: Nucleic Acids*, 3rd ed., Vol. 1, CRC Press, Boca Raton, FL.
21. Stivers, J. T. (1998) *Nucl. Acids Res. 26*, 3837−3844.
22. Lindahl, T., Ljungquist, S., Siegert, W., Nyberg, B., & Sperens, B. (1977) *J. Biol. Chem. 252*, 3286−3294.
23. Mazumder, A., Gerlt, J. A., Rabow, L., Absalon, M. J., Stubbe, J., & Bolton, P. H. (1989) *J. Am. Chem. Soc. 111*, 8029−8030.
24. Kuzmic, P. (1996) *Anal. Biochem. 237*, 260−273.

25. Johnson, K. A. (1992) in *The Enzymes*, Vol. XX, pp 1−61, Academic Press, Orlando, FL.
26. Fierke, C. A., & Hammes, G. G. (1995) *Methods Enzymol. 249*, 3−37.
27. Leatherbarrow, R. J. (1998) *GraFit 4.0*, Erithacus Software Ltd., Staines, U.K.
28. Barshop, B. A., Wrenn, R. F., & Frieden, C. (1983) *Anal. Biochem. 130*, 134.
29. Zimmerle, C. T., & Freiden, C. (1989) *Biochem J. 258*, 381−387.
30. Scharer, O. D., Kawate, T., Gallinari, P., Jiricny, J., & Verdine, G. L. (1997) *Proc. Natl. Acad. Sci. U.S.A. 94*, 4878−4883.
31. Millar, D. P. (1996) *Curr. Opin. Struct. Biol. 6*, 322−326.
32. Stivers, J. T., Pankiewicz, K. W., & Watanabe, K. A. (1998) *FASEB J. 12*, Abs. 248, A1353.
33. Williams, D. M., Benseler, F., & Eckstein, F. (1991) *Biochemistry 30*, 4001−4009.
34. Varshney, U., & van de Sande, J. H. (1991) *Biochemistry 30*, 4055−4061.
35. Panyatou, G., Brown, T., Barlow, T., Pearl, L. H., & Saava, R. (1998) *J. Biol. Chem. 273*, 45−50.
36. Fersht, A. (1985) *Enzyme Structure and Mechanism*, pp 150−151, W. H. Freeman and Co., New York.
37. Mullen, G. P., & Wilson, S. H. (1997) *Biochemistry 36*, 4713−4717.
38. Verdine, G. L., & Bruner, S. D. (1997) *Chem. Biol. 4*, 329−334.
39. Higley, M., & Lloyd, R. S. (1993) *Mutat. Res. 294*, 109−116.
40. Purmal, A. A., Lampman, G. W., Pourmal, E. I., Melamede, R. J., Wallace, S. S., & Kow, Y. W. (1994) *J. Biol. Chem. 269*, 22046−22053.
41. Bennett, S. E., Sanderson, R. J., & Mosbaugh, D. W. (1995) *Biochemistry 34*, 6109−6119.
42. von Hippel, P. H., & Berg, O. G. (1989) *J. Biol. Chem. 264*, 675−678.
43. Berg, O. G., Winter, R. B., & von Hippel, P H. (1981) *Biochemistry 20*, 6926−6948.
44. Lycksell, P. O., Graslund, A., Claesens, F., McLaughlin, L. W., Larsson, U., & Rigler, R. (1987) *Nucleic Acids Res. 15*, 9011−9025.
45. Gueron, M., Kochoyan, M., & Leroy, J. L. (1987) *Nature 328*, 89−92.
46. Benight, A. S., Schurr, J. M., Flynn, P. F., Reid, B. R., & Wemmer, D. E. (1988) *J. Mol. Biol. 184*, 165−178.
47. Brooks, B., & Benisek, W. F. (1994) *Biochemistry 33*, 2682−2687.
48. Barrett, T. E., Savva, R., Panayatou, G., Barlow, T., Brown, T., Jiricny, J., & Pearl, L. (1998) *Cell 92*, 117−129.

BI9818669